

Assessment of Alterations in the Electrical Impedance of Muscle After Experimental Nerve Injury via Finite-Element Analysis

Lucy L. Wang, Mohammad Ahad, Alistair McEwan, Jia Li, Mina Jafarpoor, and Seward B. Rutkove*

Abstract—The surface measurement of electrical impedance of muscle, incorporated as the technique of electrical impedance myography (EIM), provides a noninvasive approach for evaluating neuromuscular diseases, including amyotrophic lateral sclerosis. However, the relationship between alterations in surface impedance and the electrical properties of muscle remains uncertain. In order to investigate this further, a group of healthy adult rats, a group of rats two weeks postsciatic crush, and a group of animals six months postcrush underwent EIM of the gastrocnemius–soleus complex. The animals were then killed and the conductivity and permittivity of the extracted muscle measured. Finite-element models based on MRI data were then constructed for each group. The characteristic EIM parameter, 50 kHz phase (\pm standard error), obtained with surface impedance measurements was $17.3^\circ \pm 0.3^\circ$ for normal animals, $13.8^\circ \pm 0.7^\circ$ for acutely injured animals, and $16.1^\circ \pm 0.5^\circ$ for chronically injured animals. The models predicted parallel changes with phase values of 24.3° , 18.8° , and 21.2° for the normal, acute, and chronic groups, respectively. Other multifrequency impedance parameters showed similar alterations. These results confirm that surface impedance measurements taken in conjunction with anatomical data and finite-element models may offer a noninvasive approach for assessing biophysical alterations in muscle in neuromuscular disease states.

Index Terms—Element methods, impedance, muscle.

I. INTRODUCTION

THE SURFACE measurement of electrical impedance over localized areas of muscle can provide a noninvasive means for evaluating diseases of both peripheral nerve and muscle [1]. To date, this approach, defined as the technique of electrical impedance myography (EIM), has been used directly to study human subjects with radiculopathy, amyotrophic lateral sclerosis, myositis, spinal muscular atrophy, and muscle atrophy due

to disuse injury [2]–[6]. The main purpose of these measurements has not been to attempt to diagnose the conditions, but rather as a noninvasive means for assessing disease status. Such a measure of disease status can be extremely important in therapeutic treatment trials since it has the potential of providing a very sensitive measure of drug effect not easily identified with more standard approaches such as muscle strength or physical function testing. It also remains possible that similar to standard needle electromyography (EMG), EIM can provide basic insights into disease origin, including whether a disease is primarily caused by nerve or muscle injury [7].

The parameters assessed in EIM include the measured resistance (R), the reactance (X), and the phase angle (θ). The alterations in the surface electrical impedance data that occur with disease are undoubtedly related to a number of factors, including a combination of gross geometric alterations (e.g., changes in muscle volume and shape) and microscopic alterations, shifts in the dielectric properties of the tissue itself due to loss/gain of water or fat, and changes in shape and organization at the cellular level. Studying the relationship between surface impedance values and tissue pathology directly in human subjects would be difficult, and thus, we have initiated a program of reverse translational research focused on measuring these alterations in rodent disease models. After surface impedance data are collected on a given disease model, the animal is sacrificed and direct measurement of the electrical properties of the muscle in an impedance cell is performed; the tissue can also then be evaluated by using quantitative microscopic techniques [8].

An appealing approach for assessing these disease-induced alterations is via the finite-element method since it can simultaneously incorporate alterations in both muscle geometry and the electrical characteristics of the tissue [9]. In this study, we build upon our preliminary study by performing a series of measurements and subsequent analyses relying upon sciatic nerve crush, the standard model for muscle denervation. Here, we assess animals at 1–2 weeks after injury, when they are expected to be most severely denervated, and at six months, when reinnervation of the muscle has long been completed [10]. We also compare both groups to a cohort of healthy animals of similar age. If surface EIM data can be reproduced and confirmed by using the model, it may be possible to attempt to reverse-calculate dielectric properties from known surface EIM values. Although such an approach has substantial challenges as it requires the solution to an ill-posed inverse problem [11], if successful, it could provide data on pathological changes without the need

Manuscript received August 25, 2010; revised November 24, 2010; accepted December 17, 2010. Date of publication January 10, 2011; date of current version May 18, 2011. This work was supported in part by the National Institutes of Health under Grant R01NS055099. *Asterisk indicates corresponding author.*

L. L. Wang, M. Ahad, J. Li, and M. Jafarpoor are with the Department of Neurology, Beth Israel Deaconess Medical Center, Boston, MA 02115 USA (e-mail: llwang@bidmc.harvard.edu; mahad@georgiasouthern.edu; jli9@bidmc.harvard.edu; mjafarpoor@bidmc.harvard.edu).

A. McEwan is with the Department of Electrical and Information Engineering, University of Sydney, Sydney, NSW 2006, Australia (e-mail: alistair.mcewan@sydney.edu.au).

*S. B. Rutkove is with the Department of Neurology, Beth Israel Deaconess Medical Center, Boston, MA 02115 USA (e-mail: srutkove@bidmc.harvard.edu).

Digital Object Identifier 10.1109/TBME.2011.2104957

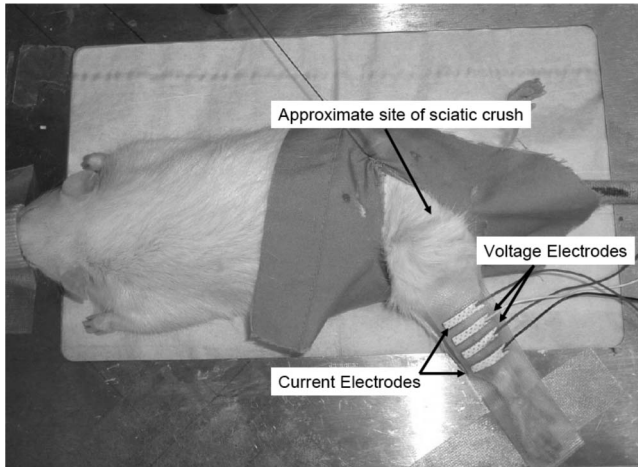


Fig. 1. Experimental setup, showing location of the current injecting and voltage measuring electrodes overlying the gastrocnemius muscle; the approximate site of the sciatic nerve crush is also shown. The muscle is extracted from directly below the four-electrode array.

to employ invasive techniques such as muscle biopsy or needle EMG.

II. METHODS

A. Animals

A total of 32 male Wister rats were obtained from Charles River Laboratories, Wilmington, MA, of approximately 6–8 weeks of age. These rats were divided into three groups: 12 to undergo acute sciatic crush studies, 12 to undergo chronic sciatic crush studies, and eight as controls. All studies were approved by the Institutional Animal Care and Use Committee at Beth Israel Deaconess Medical Center.

B. EIM Measurements

EIM measurements were made as previously described [12] and as shown in Fig. 1. Briefly, Ambu Neuroline 700 surface adhesive Ag–AgCl electrodes (Product # 70010-K/C/12, AMBU, Inc., Bethesda, MD) were used to obtain EIM data. These electrodes were resized to 3.5 mm × 18 mm by using a customized razor cutter. Sets of four cut electrodes were assembled by using adhesive tape with interelectrode distances of 4 mm, yielding a standard tetrapolar array consisting of two current electrodes and two voltage measuring electrodes. The array of electrodes was applied to the shaved hind leg with the electrode axes perpendicular to the long axis of the limb [3].

Impedance data were obtained by using a multifrequency lock-in amplifier (Model 7280, Signal Recovery, Oak Ridge, TN) sampling at 7.5 MHz coupled with a very low-capacitance active probe (Model 1103 of Tektronix, Beaverton, OR). This system has a high input impedance of 1 MΩ–1 pF, three orders of magnitude greater than our measured contact impedances. Measurements were made at approximately logarithmically spaced intervals over a frequency spectrum of 0.5 to 300 kHz as previously described [12]. Prior to measurements, the system was calibrated with known resistor–capacitor elements designed to

mimic the electrical properties of muscle to be encountered in the planned measurements.

By using the EIM electrodes as landmarks, girth measurements were taken by using a standard measuring tape at six circumferences along the hind limb: above the placement of the electrode array near the knee joint, at each electrode placement, and at the ankle joint. Values for each locale were averaged over the individuals for each group of animals and served as the framework for the geometric model. Because of differences in age between the three groups and nerve injury status at the time of sacrifice, the sizes of the rat leg models varied accordingly.

C. Sciatic Crush

Sciatic crush surgery was performed while rats were anesthetized under 1%–3% isoflurane via a nose cone. An incision was made proximally in the left thigh and the sciatic nerve exposed (see Fig. 1). A 1 mm segment of sciatic nerve was crushed using jeweler’s forceps by applying 3–4 MPa pressure for approximately 30 s. The wound was then sutured and treated with topical antibiotic ointment. To control pain, buprenorphine was administered intraperitoneally at a dose of 0.5 mg/kg every 24 h for two days following the surgery. The animals were allowed to recover until their predetermined date of measurement and subsequent sacrifice.

D. Dielectric Measurements and Calculations

Both longitudinal and transverse dielectric measurements over the same 0.5–300 kHz frequency range were made on a 1 cm × 1 cm × 0.5 cm slab of extracted gastrocnemius muscle complex immediately after animal sacrifice, as previously described [8]. Briefly, a custom-designed measuring cell with base dimension 1 cm × 1 cm and height 2 cm was used for these measurements. Specific to the cell was a lid with four small boreholes spaced 2 mm apart in a row and 2 mm away from the edges of the cell. Two thin metal plates of 1 cm × 5 cm were mounted on opposing sides of the cell and served as current electrodes. Two monopolar EMG needle electrodes (Ref# 902-DMG50, Viasys Healthcare) were inserted into the holes on the lid to serve as voltage measuring electrodes. Distances of 4 and 6 mm between voltage electrodes were used for subsequent measurements.

The conductivity (σ) and relative permittivity (ϵ_r) of the tissue were calculated by the following two equations:

$$\sigma = KG = \frac{d}{A} \times \frac{R}{R^2 + X^2} \quad (1)$$

$$\epsilon_0 \epsilon_r = KC = \frac{d}{A} \times \frac{X}{\omega(R^2 + X^2)} \quad (2)$$

where the conductance $G = R/(R^2 + X^2)$, the capacitance $C = X/(\omega(R^2 + X^2))$, and the geometry factor $K = d/A$ (and R is the measured resistance, X the measured reactance, ω the applied frequency, d the distance between voltage electrodes, A the cross-sectional area of the muscle, and ϵ_0 the permittivity of free space).

For the geometry factor K , cross-sectional area A was calculated by using the height of the muscle and the $1\text{ cm} \times 1\text{ cm}$ basal area. The raw impedance data were obtained by using the two electrode distances (6 and 4 mm) that were averaged together for each muscle in the longitudinal and transverse directions. Resistance and reactance values were used to extract the dielectrics for each individual rat. Conductivities and permittivities were then averaged over each group of animals.

E. MRI

In order to develop an accurate finite-element model with all of the tissue compartments correctly placed and sized, one animal underwent MRI. A 4.7 T system (BioSpec 47/40; Bruker Biospin, Billerica, MA) with a transmit/receive birdcage coil (inner diameter, 72 mm) was used. Measurements were made with the animal under 1%–3% isoflurane anesthesia via a nose cone in a prone position, with the leg centered in the coil. The leg was fixed in a position identical to that which was used when performing EIM, and the center of the electrodes array was marked using a small vial of water. Cross-sectional MRI images were obtained by using a spin echo pulse sequence (repetition time (TR) = 2200 ms, echo time (TE) = 23 ms, field of view (FOV) = $6.5 \times 6.5\text{ cm}^2$, matrix size = 256×56 , NEX = 2, slice thickness = 1 mm).

F. Finite-Element Model Development

The shape and constituents of the model were constructed by using girth measurements and MRI images of the rat hind leg. The averaged girth values for each of the three groups were used to construct the backbone of the model that provides distinctions in size and convexity of the limb. In the two diseased models (acute and chronic sciatic crush), the reduced girth was translated into a reduced volume of the muscle compartments, while keeping the other components of the model (e.g., skin-subcutaneous fat and bone) unchanged. The two ends of the model were established by using the average knee and ankle girth measurements, and the circumference of the muscle bulk by using the remaining girth measurements, thus accounting for the geometrical differences between the three groups of animals.

The model extended from the knee to ankle joint and consisted of a skin/subcutaneous fat layer, a fascia layer, two bones (tibia and fibula), and several regions of muscle: the biceps femoris (see Fig. 2), the gastrocnemius–soleus complex, and the tibialis anterior. The biceps femoris and tibialis anterior were given characteristic small angles α and β , respectively, to represent the slight offset in muscle fiber direction from parallel. The final angles used to obtain the multifrequency solution were $\alpha = 5^\circ$ and $\beta = 5^\circ$ relative to the long axis of the limb (i.e., the cylinder). Subcutaneous fat was estimated to be approximately 1 mm thick throughout, and the fascial layer 0.5 mm. Electrodes were modeled based on the strip electrodes used in EIM, measuring $3.5\text{ mm} \times 18\text{ mm}$ individually with 4 mm interelectrode distance. Only the metallic surface of the electrode was modeled; no interelectrode capacitances or contact impedances were included in the model (the latter due to the fact that these are inconsequential being several orders of magnitude smaller

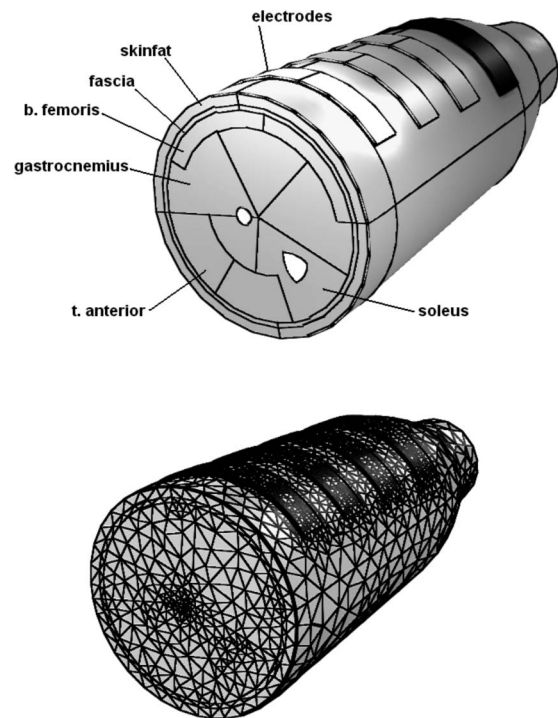


Fig. 2. (Above) FEM model of chronic crush rat hind leg as constructed based on MRI images. The major muscle complexes, bones, and surface structures are represented. (Below) Mesh, consisting of 54 365 triangular elements.

than the input impedance of the voltage sensors). The muscle groups and tissue constituencies were consistent across the models developed for each of the three groups of animals, and key differences were accounted for by varying girth. Comsol Multiphysics software (Comsol, Inc., 3.4 Burlington, MA), ac/dc module, quasi-statics were used in this analysis [13]. The final meshes for the three models consisted of 49 360–54 365 triangular elements.

The normal component of the current between two adjoining tissue compartments was assumed to be continuous and no current flow out of any exterior boundaries of the model was included; the latter is a reasonable assumption since the skin, knee, and ankle bones at both ends are relatively poor conductors. Because a substantial part of the hind limb was modeled on either side of the electrode array, the shifts in results arising from current escape were expected to be minimal.

At each frequency, mean longitudinal and transverse conductivity and permittivity values for muscle for the group of animals were incorporated based on the dielectric measurements of the rat muscle. Skin–subcutaneous fat and fascia values were obtained over the frequency spectrum from Gabriel's dielectric survey and the associated online resources [14], [15]. Both subcutaneous fat and fascia were assumed to be isotropic, with consistent conductivity values over the multifrequency spectrum. The subcutaneous fat conductivity was set to 0.03 S/m and the fascia conductivity to 0.2 S/m. Relative permittivities, being more frequency-dependent, were incorporated over the frequency spectrum [5]. For bone, conductivity was set to 0.02 S/m and relative permittivity to 6000. The electrodes were assigned conductivity $5.0\text{e}5\text{ S/m}$ and relative permittivity 1.0.

In order to assess the accuracy in the value of the electrode parameters, the same model was solved by using 1.0×10^{-3} times the conductivity of the electrodes, which yielded that overall predicted surface impedance increases over the entire frequency spectrum of only $<0.1 \Omega$ resistance and reactance. After solving the finite-element problem, the voltage at the midpoint of both inner electrodes was assessed and the surface resistance and reactance values extracted.

G. Data Analysis

All dielectric values and characteristic EIM values are presented as the average of individuals in each group with the standard error of the mean (SEM). The conductivity and permittivity values of individuals averaged per group were used as the dielectric inputs of their respective models. Averaged dielectrics were used to solve for surface voltages at frequencies between 0.5 and 300 kHz, with ten frequencies per decade.

For EIM, 50 kHz resistance, reactance, and phase were used as characteristic comparative quantities. This choice was largely based on its and demonstrated value in the previous study [3], [12], [16] and the abundance of commercial devices available for impedance measurements at this single frequency. In addition to single-frequency data, we also calculated three “collapsed” multifrequency parameters: the logRslope (calculated by performing a log–log transformation on the resistance data from 10 to 300 kHz and taking the slope of a fitted linear regression), the reactance slope (the slope of a linear regression taken from the descending portion of the multifrequency spectrum from 100 to 300 kHz), and phase slope (the slope of a linear regression taken from 100 to 300 kHz spectrum of phase). In this paper, these summary measures of the multifrequency data have been valuable in quantifying neuromuscular disease severity [5].

III. RESULTS

Due to postsurgical complications or other technical complications, data could not be obtained from four animals, one in the acute crush group and three in the chronic crush group. Thus, the results next are based on data from 11 animals in the acute group and nine in the chronic group. Normal measurements are presented as an average of the eight animals in the control group.

The measured mean \pm SEM 50 kHz longitudinal and transverse conductivities and permittivities for the three groups of animals are shown in Table I. As an internal check on the precision of our measurements, we also compared the calculated conductivity and permittivity values for the two distances in the impedance cell; for conductivity, the values varied, on average, by $16.0\% \pm 5.5\%$, and for permittivity, they varied, on average, by $15.7\% \pm 3.3\%$.

By using this mean dielectric data and the basic model shown in Fig. 2, surface impedance values were calculated over frequencies 0.5–300 kHz for each of the three groups: normal, acute crush, and chronic crush. The finite-element models were constructed by using unique girth values, with differing volumes of the overall muscle component.

For comparison, average girth around the center point of the electrode array was 6.10 ± 0.11 cm for controls, 5.65 ± 0.13 cm

TABLE I
CONDUCTIVITY AND PERMITTIVITY VALUES OF RAT MUSCLE AT SELECTED FREQUENCIES

Normal				
Freq.	σ_L (S/m)	σ_T (S/m)	ϵ_L	ϵ_T
10000	0.39 \pm 0.06	0.12 \pm 0.01	146877 \pm 16526	94162 \pm 8158
25000	0.44 \pm 0.082	0.15 \pm 0.014	96105 \pm 13335	74317 \pm 5100
50000	0.51 \pm 0.067	0.2 \pm 0.018	70461 \pm 2051	56514 \pm 3874
100000	0.52 \pm 0.063	0.28 \pm 0.024	36556 \pm 5257	35936 \pm 2279
150000	0.6 \pm 0.068	0.35 \pm 0.024	41945 \pm 4017	27337 \pm 1195
300000	0.72 \pm 0.074	0.47 \pm 0.024	13214 \pm 1455	14877 \pm 1097
Acute Crush				
Freq.	σ_L (S/m)	σ_T (S/m)	ϵ_L	ϵ_T
10000	0.5 \pm 0.04	0.14 \pm 0.01	104370 \pm 7160	80869 \pm 2012
25000	0.55 \pm 0.037	0.16 \pm 0.013	64132 \pm 4486	62571 \pm 1479
50000	0.59 \pm 0.039	0.2 \pm 0.013	41997 \pm 2814	49670 \pm 1070
100000	0.64 \pm 0.041	0.27 \pm 0.013	26394 \pm 1715	36123 \pm 849
150000	0.68 \pm 0.043	0.33 \pm 0.013	19875 \pm 1469	28671 \pm 722
300000	0.75 \pm 0.046	0.46 \pm 0.014	12277 \pm 1072	17514 \pm 564
Chronic Crush				
Freq.	σ_L (S/m)	σ_T (S/m)	ϵ_L	ϵ_T
10000	0.52 \pm 0.074	0.15 \pm 0.016	126661 \pm 14523	102352 \pm 10378
25000	0.61 \pm 0.070	0.18 \pm 0.022	80369 \pm 9623	78265 \pm 7845
50000	0.65 \pm 0.063	0.23 \pm 0.027	55771 \pm 4475	59379 \pm 3912
100000	0.73 \pm 0.062	0.32 \pm 0.045	35184 \pm 2705	44217 \pm 3841
150000	0.77 \pm 0.063	0.38 \pm 0.041	25410 \pm 1777	33063 \pm 2215
300000	0.82 \pm 0.076	0.53 \pm 0.047	14347 \pm 1577	19308 \pm 1583

Freq. is the frequency; σ_L the longitudinal conductivity; σ_T the transverse conductivity; ϵ_L the longitudinal relative permittivity; and ϵ_T the transverse relative permittivity.

for acute sciatic crush, and 6.3 ± 0.15 cm for chronic sciatic crush. EIM measurements and finite-element method (FEM) predictions for the 50 kHz impedance values (resistance, reactance, and phase) are compared in Table II. In general, calculation of impedances by using finite-element analysis finished after approximately 20 s within $1 \times 10^{-3} \Omega$ of the convergence limit. Each 50 kHz EIM parameter showed a shift away from baseline in the acute group. The chronic group had surface impedance values similar to the normal group. Because of the six-month postsurgery period, these chronic crush animals presumably had experienced reinnervation to a measurable degree in all but the most injured animals, and this shift back to normal was thus expected.

Fig. 3 provides the multifrequency spectrum for all three groups, comparing the predicted multifrequency data of resistance, reactance, and phase to the surface-measured EIM values.

In order to summarize the behavior of the entire spectrum with varying degrees of severity, we also utilize the collapsed parameters described in Section II-G earlier. These results in addition to the 50 kHz measures are shown in Fig. 4 in which the predicted values are displayed directly below the measured

TABLE II
COMPARISON BETWEEN EIM-MEASURED VALUES AND FEM MODEL PREDICTIONS AT 50 KHZ

<i>EIM</i>			
Value	Normal	Acute	Chronic
R50	73.3±0.9	74.2±1.9	72.7±3.2
X50	22.8±0.2	18.2±0.6	21.2±1.2
P50	17.3±0.3	13.8±0.7	16.1±0.5

<i>FEM</i>			
Value	Normal	Acute	Chronic
R50	86.7	87.8	78.3
X50	36.7	29.9	30.3
P50	24.3	18.8	21.2

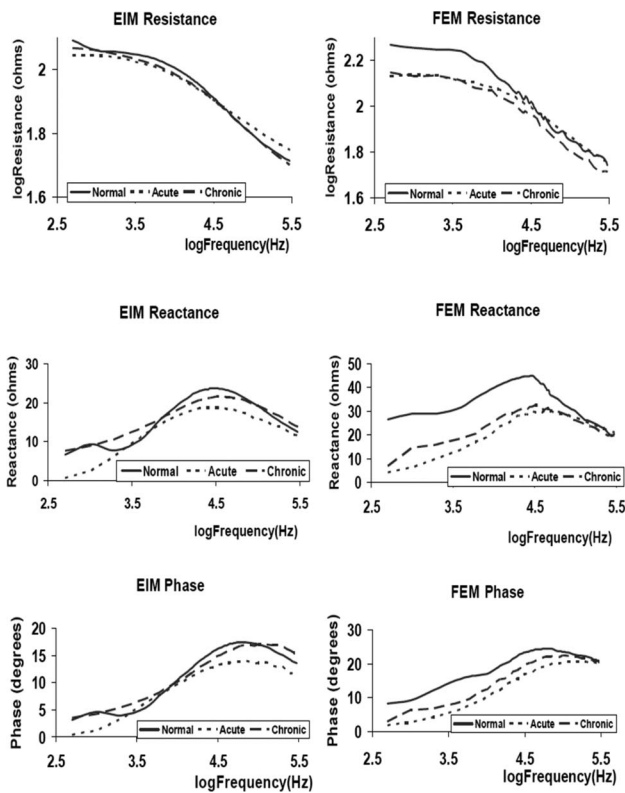


Fig. 3. Average EIM resistance, reactance, and phase next to the counterparts predicted by using finite-element modeling. Curves are plotted on different scales for EIM and FEM to highlight the relative shifts of the multifrequency spectrum between the three study groups relative to one another rather than their absolute values.

values for easy comparison. As can be seen, for the most part, the FEM predicted outcomes for these EIM measures parallel those results obtained with surface measurement, with the two notable exceptions being the 50 kHz reactance for the chronic crush animals and the phase slope for the acute crush animals. In all other measures, the FEM-collapsed parameters show a greater shift between acute and normal than between chronic and normal, consistent with the measured data. In short, although the absolute values often vary considerably at 50 kHz, our model

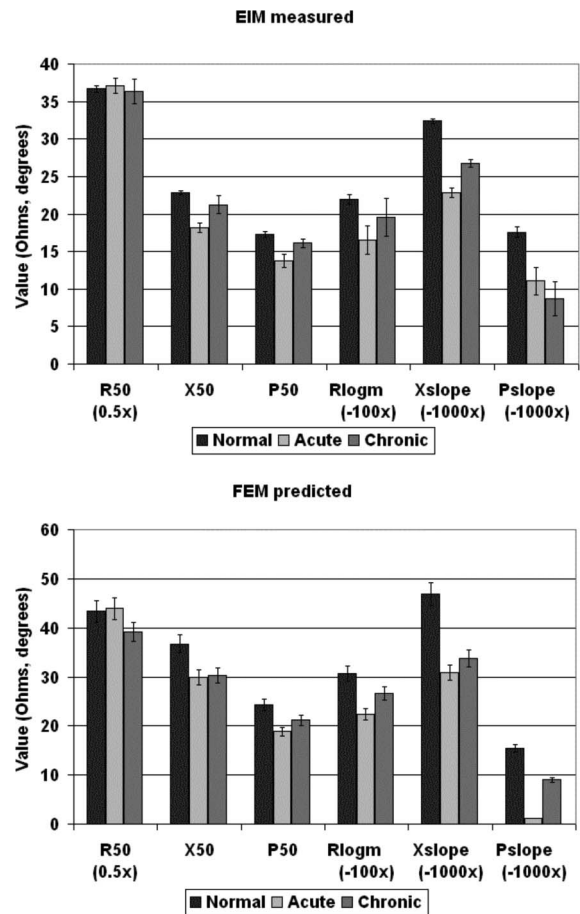


Fig. 4. (Above) Comparative bar chart of measured EIM parameters in normal, acute, and chronic crush animals, with standard errors. The relative position of the three groups is apparent. (Below) FEM predicted values for the five parameters, plotted with 5% error bars, show similar relationships, especially in log-resistance slope, reactance slope, and 50 kHz phase. Scales of parameters have been adjusted to be displayed on the same plot, with error tolerance similarly adjusted.

correctly predicts the direction and relative magnitude of the changes for most of the parameters assessed.

IV. DISCUSSION

By using approximated muscle geometry and immediately postmortem dielectric values, finite-element analysis predicts to reasonable extent changes in the surface-acquired EIM data. Because a different model was constructed for each group (normal, acute crush, and chronic crush), based on differences in girth, the geometric contribution to the surface data, we believe, has largely been accounted for. This indicates that the observed alterations in the surface-acquired data are providing, in part, information about the muscle's underlying electrical properties.

Even though the relative relationships between normal, acute, and chronic crush tissue were obtained by using FEM paralleled alterations in the surface recorded data, the actual values differed considerably at 50 kHz by about 15% for resistance, 60% for reactance, and 30% for the calculated phase at 50 kHz. The reactance values being considerably smaller in the magnitude than the resistance values had greater error. Also, as shown in Fig. 3,

there is an additional variation across the frequency range studied for each measure. There are likely several contributors to these inconsistencies. First, a likely major source of error is the accuracy of the measured tissue conductivity and permittivity values. These values are highly sensitive to temperature, moisture, and tissue quality after death, muscle size, cross-sectional area, and distance between voltage measuring electrodes during measurement. For example, it is difficult to ascertain the exact tissue dimensions, and as such the closest approximation to a 1 cm \times 1 cm base size is gauged by careful measurement with a ruler; variation of up to approximately 0.5 mm in any one direction is likely. The size of the tissue is especially important since slight distortion of the tissue, as it is placed into the impedance cell, is unavoidable, thus impacting the exact longitudinal and transverse values. In addition, we did control temperature with a heating lamp and heating pad underneath the measurement cell, but temperature variation of up to 2 °C was unavoidable. Perhaps, most importantly, these impedance cell measurements by necessity are conducted on dead tissue. Even though these measurements are made within 10 min of animal sacrifice, alteration in the measured conductivity and relative permittivity is bound to occur.

In addition, the model itself has a variety of assumptions and inaccuracies. First, it uses skin, subcutaneous fat, and fascia dielectric values from Gabriel *et al.*'s and the associated online resources [14], [15] that are based on sheep data; no doubt, these values likely differ from those of the rodents. Indeed, our 50 kHz conductivity and permittivity values for muscle in the longitudinal direction (0.46 S/m and 56 330, respectively) are far from those obtained from the online resource (0.34 S/m and 10 094). Obtaining actual fat, bone, and fascia data from the rat directly, however, would be difficult in the extreme given the animals' small size. Evens so, shifts in these values will undoubtedly impact the results. To test this idea, we arbitrarily reduced the subcutaneous fat conductivity by 10% from that obtained from Gabriel at 50 kHz. This resulted in a 0.2% reduction in predicted surface resistance, a 4.9% reduction in predicted surface reactance, and a 3.9% reduction in predicted surface phase. A second confounding problem is that of the biceps femoris and tibialis anterior muscles. These muscles run at an oblique angle relative to the long axis of the limb. In the model used here, they were placed at 5° relative to the major fiber direction of the gastrocnemius–soleus; small inaccuracies in this angle will also influence the results of the model.

To date, much of our study on studying electrical impedance alteration in muscle has been based on phenomenological relationships, such as correlating the degree of weakness in a given muscle and the alteration in the surface-measured impedance of muscle [4], [5]. Although we have been able to identify substantial alterations in the measured impedance, the mechanism by which these alterations occur are undoubtedly multifactorial, likely being related to both volume loss/geometric change and alterations in the electrical properties of the muscle itself. Our ability to identify alterations in the raw conductivity and relative permittivity values and demonstrate their relationship to surface-recorded values strengthens the argument for attempting to pursue inverse modeling, incorporating basic anatomic/geometric

considerations, and FEM to approximate the underlying electrical properties of the tissues directly. Although clearly a challenging proposition given its nature as an ill-posed inverse problem, further investigation in this direction is warranted. Ultimately, measuring surface impedance and basic limb shape could potentially allow us to quantify the status of the underlying muscle tissue, and thus, noninvasively obtain new information about the status of diseased muscle in human subjects. Such modeling could assist in not only in assessing disease type (for example, distinguishing myopathic from neurogenic disorders), but also in assessing disease severity.

A logical extension of this basic approach is also to incorporate measurement of muscle anisotropy. Indeed, alterations in muscle anisotropy may provide a unique window into disease status since we have already identified major changes in surface anisotropy in neuromuscular disease patients [1]. Measurement of this property, however, has been limited by the absence of devices geared specifically for the measurement of surface anisotropy although a recently developed system [17] is now allowing us to do just that. The study completed here provides a first step toward that realization.

ACKNOWLEDGMENT

The authors would like to thank M. Fogerson for the valuable assistance in the completion of this paper.

REFERENCES

- [1] S. B. Rutkove, "Electrical impedance myography: Background, current state, and future directions," *Muscle Nerve*, vol. 40, pp. 936–946, 2009.
- [2] S. B. Rutkove, G. Esper, K. Lee, R. Aaron, and C. A. Shiffman, "Electrical impedance myography in the detection of radiculopathy," *Muscle Nerve*, vol. 32, pp. 335–341, 2005.
- [3] S. B. Rutkove, H. Zhang, D. A. Schoenfeld, E. M. Raynor, J. M. Shefner, M. E. Cudkowicz, A. B. Chin, R. Aaron, and C. A. Shiffman, "Electrical impedance myography to assess outcome in amyotrophic lateral sclerosis clinical trials," *Clin. Neurophysiol.*, vol. 118, pp. 2413–2418, 2007.
- [4] A. W. Tarulli, G. J. Esper, K. S. Lee, R. Aaron, C. A. Shiffman, and S. B. Rutkove, "Electrical impedance myography in the bedside assessment of inflammatory myopathy," *Neurology*, vol. 65, pp. 451–452, 2005.
- [5] S. B. Rutkove, J. M. Shefner, M. Gregas, H. Butler, J. Caracciolo, C. Lin, P. M. Fogerson, P. Mongiovi, and B. T. Darras, "Characterizing spinal muscular atrophy with electrical impedance myography," *Muscle Nerve*, vol. 42, no. 6, pp. 915–921, Dec. 2010.
- [6] A. W. Tarulli, N. Duggal, G. J. Esper, L. P. Garmirian, P. M. Fogerson, C. H. Lin, and S. B. Rutkove, "Electrical impedance myography in the assessment of disuse atrophy," *Arch. Phys. Med. Rehabil.*, vol. 10, pp. 1806–1810, 2009.
- [7] L. P. Garmirian, A. B. Chin, and S. B. Rutkove, "Discriminating neurogenic from myopathic disease via measurement of muscle anisotropy," *Muscle Nerve*, vol. 39, pp. 16–24, 2009.
- [8] M. A. Ahad, P. M. Fogerson, G. D. Rosen, P. Narayanaswami, and S. B. Rutkove, "Electrical characteristics of rat skeletal muscle in immaturity, adulthood and after sciatic nerve injury, and their relation to muscle fiber size," *Physiol. Meas.*, vol. 30, pp. 1415–1427, 2009.
- [9] M. A. Ahad and S. B. Rutkove, "Finite element analysis of electrical impedance myography in the rat hind limb," in *Proc. IEEE Conf. Eng. Med. Biol. Soc.*, 2009, pp. 630–633.
- [10] M. Bendszus, C. Wessig, L. Solymosi, K. Reiners, and M. Koltzenburg, "MRI of peripheral nerve degeneration and regeneration: Correlation with electrophysiology and histology," *Exp. Neurol.*, vol. 188, pp. 171–177, 2004.
- [11] W. R. Lionheart, "EIT reconstruction algorithms: Pitfalls, challenges and recent developments," *Physiol. Meas.*, vol. 25, pp. 125–142, 2004.

- [12] M. A. Ahad and S. B. Rutkove, "Electrical impedance myography at 50 kHz in the rat: Technique, reproducibility, and the effects of sciatic injury and recovery," *Clin. Neurophysiol.*, vol. 120, pp. 1534–1538, 2009.
- [13] *User's Guide*, Comsol Multiphysics, Comsol AB, Stockholm, Sweden, 2007, 2011.
- [14] C. Gabriel, S. Gabriel, and E. Corthout, "The dielectric properties of biological tissues: I. Literature survey," *Phys. Med. Biol.*, vol. 41, pp. 2231–2249, 1996.
- [15] Institute of Applied Physics (IFAC). Dielectric properties of body tissues. (2007). [Online]. Available: <http://niremf.ifac.cnr.it/tissprop/>.
- [16] S. B. Rutkove, P. M. Fogerson, L. P. Garmirian, and A. W. Tarulli, "Reference values for 50-kHz electrical impedance myography," *Muscle Nerve*, vol. 38, pp. 1128–1132, 2008.
- [17] O. T. Ogunnika, S. B. Rutkove, H. Ma, P. M. Fogerson, M. Scharfstein, R. C. Cooper, and J. L. Dawson, "A portable system for the assessment of neuromuscular diseases with electrical impedance myography," *J. Med. Eng. Technol.*, vol. 35, pp. 377–385, 2010.

Author's photograph and biography not available at the time of publication.